PB85-138196

Evaluation of Two Numerical Integrator Schemes

Brookhaven National Lab., Upton, NY

Prepared for

Environmental Protection Agency
Research Triangle Park, NC

Dec 84

U.S. Department of Commerce
National Technical Information Service
NTIS

PB85-138196

EPA-600/3-84-112
December 1984

EVALUATION OF TWO NUMERICAL INTEGRATOR SCHEMES

by

A.A.N. Patrinos and M.J. Leach
Atmospheric Sciences Division
Department of Applied Science
Brookhaven National Laboratory
Upton, New York 11973

IAG - DW930067-01

Project Officer

Francis S. Binkowski
Meteorology and Assessment Division
Environmental Sciences Research Laboratory
Research Triangle Park, North Carolina 27711

ATMOSPHERIC SCIENCES RESEARCH LABORATORY
OFFICE OF RESEARCH AND DEVELOPMENT
U.S. ENVIRONMENTAL PROTECTION AGENCY
RESEARCH TRIANGLE PARK, NORTH CAROLINA 27711

REPRODUCED BY
NATIONAL TECHNICAL
INFORMATION SERVICE
U.S. DEPARTMENT OF COMMERCE
SPRINGFIELD, VA. 22161

TECHNICAL REPORT DATA
(Please read Instructions on the reverse before completing)

1. REPORT NO.	2.	3. RECIPIENT'S ACCESSION NO.
EPA-600/3-84-112		PB85-138196

4. TITLE AND SUBTITLE	5. REPORT DATE
EVALUATION OF TWO NUMERICAL INTEGRATOR SCHEMES	December 1984
	6. PERFORMING ORGANIZATION CODE
7. AUTHOR(S)	8. PERFORMING ORGANIZATION REPORT NO.
A.A.N. Patrinos and M.J. Leach	
9. PERFORMING ORGANIZATION NAME AND ADDRESS	10. PROGRAM ELEMENT NO.
Brookhaven National Laboratory Upton, New York 11973	CCVN1A/01-3108 (FY-84)
	11. CONTRACT/GRANT NO.
	DW930067-01
12. SPONSORING AGENCY NAME AND ADDRESS	13. TYPE OF REPORT AND PERIOD COVERED
Atmospheric Sciences Research Laboratory--RTP, NC Office of Research and Development U.S. Environmental Protection Agency Research Triangle Park, NC 27711	Final
	14. SPONSORING AGENCY CODE
	EPA/600/09

15. SUPPLEMENTARY NOTES

16. ABSTRACT

Two numerical integrators of the advection-diffusion equation used in air pollution simulations were tested in the framework of an evaluation methodology. The schemes were an integrator based on a polynomial approximation algorithm and a version of the pseudospectral integrator. The evaluation methodology included two test cases: the transport of a spline puff and a constant point source. Testing criteria included accuracy, conservation, and efficiency. Accuracy was assessed with the use of "norms" which used the exact analytical solution values.

The "polynomial" integrator demonstrated superior consistency in its performance and generally better accuracy. The cost was, however, ~2.5 times that of the pseudospectral one. The pseudospectral integrator with its expanding mesh displayed deteriorating accuracy whenever the signal approached the boundaries. Simple filtering algorithms have failed to effectively control this problem.

17. KEY WORDS AND DOCUMENT ANALYSIS

a. DESCRIPTORS	b. IDENTIFIERS/OPEN ENDED TERMS	c. COSATI Field/Group

18. DISTRIBUTION STATEMENT	19. SECURITY CLASS *(This Report)*	21. NO. OF PAGES
RELEASE TO PUBLIC	UNCLASSIFIED	43
	20. SECURITY CLASS *(This page)* UNCLASSIFIED	22. PRICE

EPA Form 2220-1 (9-73)

NOTICE

The information in this document has been funded wholly or in part by the United States Environmental Protection Agency under Interagency Agreement Number DW930067-01 to Brookhaven National Laboratory. It has been subject to the Agency's peer and administrative review, and it has been approved for publication as an EPA document. Mention of trade names or commercial products does not constitute endorsement or recommendation for use.

ABSTRACT

Two numerical integrators of the advection-diffusion equation used in air pollution simulations were tested in the framework of an evaluation methodology. The schemes were an integrator based on a polynomial approximation algorithm and a version of the pseudospectral integrator. The evaluation methodology included two test cases: the transport of a spline puff and a constant point source. Testing criteria included accuracy, conservation, and efficiency. Accuracy was assessed with the use of "norms" which used the exact analytical solution values.

The "polynomial" integrator demonstrated superior consistency in its performance and generally better accuracy. The cost was, however, ~2.5 times that of the pseudospectral one. The pseudospectral integrator with its expanding mesh displayed deteriorating accuracy whenever the signal approached the boundaries. Simple filtering algorithms have failed to effectively control this problem.

ACKNOWLEDGMENTS

The authors wish to thank Dr. R. G. Lamb of ASRL-EPA for helpful suggestions in the development of the evaluation methodology and Professor J. L. Molyneux of the University of Rochester for his assistance in research on the pseudospectral integrator and the evaluation methodology.

CONTENTS

Abstract iii
Acknowledgments iv

1. Introduction 1

2. Two Numerical Schemes 3
   The Pseudospectral Integrator 3
   The NEROS Integrator 7

3. Evaluation Methodology and Test Cases 10
   Test Cases 11
      Single Puff 11
      Constant Point Source 14
   Performance Criteria 15
      Accuracy 15
      Conservation 16
      Efficiency 16

4. Presentation of Results 17
   Advection-Diffusion/Spline Puff 18
   Advection/Spline Puff 25
   Diffusion/Spline Puff 26
   Advection-Diffusion/Constant Source 28

5. Conclusions 32

6. References 35

1. INTRODUCTION

An impressive variety of numerical schemes exists in the scientific literature for the solution of the advective-diffusion equation for atmospheric pollutants. Since exact analytical solutions for realistic simulations are very difficult, indeed impossible, to obtain, it becomes imperative to resort to numerical approximations to the exact solutions. These approximations usually rely in substituting the partial derivatives by finite difference expressions and solving the reduced equations on a network of spatial positions (mesh) over discrete increments of time. The great variety of numerical schemes results from the many possible ways by which the derivatives may be approximated and the ways that the time sequence computations may be performed. As expected, the optimum numerical scheme depends on the particular application for which it is intended. Most schemes have strong points and drawbacks and a careful consideration of all parameters determines the approximating scheme. It is generally difficult to compare various numerical schemes in terms of their overall performance; the absence of objective criteria is the primary cause. Furthermore, quantitative estimates of the scheme's performance need to be accompanied by qualitative evaluations in order to objectively characterize the overall performance.

The reference list at the end of this report includes a number of publications with scheme comparisons. Usually these comparisons are aimed toward demonstrating the superiority of the scheme being presented. Invariably, the test cases involve the solid body rotation of a puff (gaussian, cosine hill, cone, etc.). It has been argued that this test case is the most representative since the puff should return to its original position after one full revolution and if diffusion is absent, should be exactly the initial condition. This offers a convenient setting for assessing performance in terms of departure from this initial condition. Some have also argued that this test has the additional advantage of variable advective speeds; the truth,

however, is that due to the solid body rotation the example is one of constant advective speed (Fornberg, 1975).

We have some reservations regarding the use of solid body rotation as a representative test. The fundamental reason is that the performance of the scheme at the boundaries is deemphasized since in most cases the puff never approaches the boundaries. The proposed test cases will be presented in subsequent sections.

The problem of performance evaluation of numerical schemes is an important one and is expected to intensify as regulatory needs become more acute and questions arise regarding the "best" model for various applications. The activity reported here addresses some important aspects of this evaluation methodology.

2. TWO NUMERICAL SCHEMES

Two numerical schemes have been selected for application of the evaluation methodology. Both schemes have served as numerical integrators for large photochemical models and have been considered as candidates for the large-scale "acid rain" model proposed by the EPA (NCAR, 1983). The first scheme is the one developed by R. Lamb of EPA-ESRL (Lamb, 1983), which is the integrator of the NEROS (Northeast Regional Oxidant Study) model. It may be described as a Lagrangian, upwind differencing scheme. The second scheme is a version of the pseudospectral air pollution model (Christensen and Prahm, 1976) developed at Brookhaven National Laboratory (Patrinos and Leach, 1982). It should be emphasized that the choice of these two integrators does in no way imply that they were considered the "best"; available resources precluded a wider participation of operational integrators. Furthermore, the primary objective was to investigate the evaluation methodology not to recommend the "ultimate" integrator.

THE PSEUDOSPECTRAL INTEGRATOR

The pseudospectral method for the solution of the dispersion equations is a relatively recent development (Gazdag, 1973; Fox and Orszag, 1973) which offered some advantages over the more established finite difference schemes. The main advantage is the superior accuracy in the representation of the spatial derivatives; the only limit is the extent to which a distribution can be represented on a finite set of meshpoints. The pseudospectral method is based on the expansion of the dependent variables in terms of orthogonal functions, particularly with finite Fourier series expansions due to the development of the fast Fourier transform (FFT). The penalty for the use of these expansions is the need to impose periodic boundary conditions. If the derivatives of nonperiodic functions are computed by a finite Fourier series expansion, the series is slowly convergent due to the so-called "ringing" or

Gibbs phenomenon at the boundary discontinuities (Wengle and Seinfeld, 1978). Periodic boundary conditions are unsuitable in air pollution simulations because material advected across one boundary falsely reappears across the opposite one. Some solutions to this problem have been proposed. In one case an artificial sink term in the form of an absorbing layer on the boundaries is introduced (Christensen and Prahm, 1976). Although successful, this technique sacrifices the outer grid layers. Another approach has been to expand the variables in terms of nonperiodic functions, e.g., Chebyshev polynomials (Wengle and Seinfeld, 1978). Despite modifications to utilize the FFT, this approach introduces additional complexities which increase computational times.

We have introduced an alternative solution to this problem by performing a coordinate transformation. The suggested approach is presented in a two-dimensional framework. We assume the following equation

$$\frac{\partial c}{\partial t} = - u \frac{\partial c}{\partial x} - v \frac{\partial c}{\partial y} + K \left(\frac{\partial^2 c}{\partial x^2} + \frac{\partial^2 c}{\partial y^2}\right) , \qquad (1)$$

over the infinite 2-D domain with initial conditions $c(x,y,0) = Co(x,y)$. We transform the space variables,

$$x = \tan \left(\frac{\pi}{2} \xi\right) , \; y = \tan \left(\frac{\pi}{2} \eta\right) , \qquad (2)$$

and substitute in (1) to obtain,

$$\frac{\partial c}{\partial t} = - \frac{2}{\pi} \cos^2 \left(\frac{\pi}{2} \xi\right) \left[u + K \sin(\pi\xi)\right] \frac{\partial c}{\partial \xi} - \frac{2}{\pi} \cos^2\left(\frac{\pi}{2} \eta\right)$$

$$\left[v + K \sin(\pi\eta)\right] \frac{\partial c}{\partial \eta} + \frac{4K}{\pi^2} \left[\cos^4\left(\frac{\pi}{2} \xi\right) \frac{\partial^2 c}{\partial \xi^2} + \cos^4 \left(\frac{\pi}{2} \eta\right) \frac{\partial^2 c}{\partial \eta^2}\right] , \qquad (3)$$

where $-1 \leq \xi, \eta \leq + 1$.

We now consider the pseudospectral numerical solution of (3) on a uniform mesh with grid spacing $\Delta\xi = \frac{2}{N_\xi}$ and $\Delta\eta = \frac{2}{N_\eta}$, where N_ξ and N_η are

the number of gridpoints along the ξ and η axes, respectively. Imposing the necessary periodic boundary conditions, we solve in the domain defined by $-1 \leq \xi \leq +1 - \Delta\xi$, and $-1 \leq \eta \leq +1 - \Delta\eta$.

The above transformation effectively minimizes the importance of the boundary conditions since for all practical purposes the signal never crosses the boundaries. Furthermore, it permits a spatially variable grid density with improved accuracy in the areas of great interest and deteriorating accuracy in areas of low interest for the same computational costs of a uniform accuracy simulation. This may be a desirable situation in air pollution calculations when fine resolution is required in sensitive receptor regions, while diminished accuracy may be tolerated upwind of the major sources.

Further modifications to the above transformations were prompted by the need to provide a uniform grid over some region of real space due to e.g., the presence of several important receptor regions and the desire to avoid singling out one as the most important. The designed modifications effectively created a uniform inner grid core in real space with an expanding mesh around it; the transformed mesh was, of course, uniform throughout.

One modification involved the following transformation:

$$x = \frac{\xi}{\alpha} \ , \ 0 < |\xi| \leq \alpha \ , \text{ and}$$

$$|x| = 1 + \frac{2}{\pi} \frac{1-\alpha}{\alpha} \tan\left(\frac{\pi}{2} \frac{|\xi|-\alpha}{1-\alpha}\right) \ , \ \alpha < |\xi| < 1 \ , \qquad (4)$$

with similar expressions for the y direction.

Another modification involved the following transformation:

$$x = \frac{\xi}{\alpha} \ , \ 0 < |\xi| \leq \alpha\varepsilon \ , \text{ and}$$

$$|x| = \varepsilon + \frac{2}{\pi} \frac{1-\alpha\varepsilon}{\alpha} \tan\left(\frac{\pi}{2} \frac{|\xi|-\alpha\varepsilon}{1-\alpha\varepsilon}\right) \ , \ \alpha\varepsilon < |\xi| < 1 \ , \qquad (5)$$

with similar expressions for the y direction. The parameters α and ε could be chosen depending on the particular mesh requirements and as a result of

accuracy optimization exercises. Both these transformations insure the continuity of the spatial variables and their first derivatives across the interfaces of the two meshes.

The transformed equation for case (5) is as follows:

$$\frac{\partial c}{\partial t} = -\alpha u \frac{\partial c}{\partial \xi} - \alpha v \frac{\partial c}{\partial \eta} + \alpha^2 K \left(\frac{\partial^2 c}{\partial \xi^2} + \frac{\partial^2 c}{\partial \eta^2}\right), \quad \text{for } |\xi| \leq \alpha\varepsilon, \text{ and}$$

$$\frac{\partial c}{\partial t} = -\cos^2\left(\frac{\pi}{2}\,\frac{\xi-\alpha\varepsilon}{1-\alpha\varepsilon}\right)\left[u + \frac{\pi}{2} K \frac{\alpha^2}{1-\alpha\varepsilon} \sin\left(\pi \frac{\xi-\alpha\varepsilon}{1-\alpha\varepsilon}\right)\right] \frac{\partial c}{\partial \xi} + \tag{6}$$

$$-\cos^2\left(\frac{\pi}{2}\,\frac{\eta-\alpha\varepsilon}{1-\alpha\varepsilon}\right)\left[v + \frac{\pi}{2} K \frac{\alpha^2}{1-\alpha\varepsilon} \sin\left(\pi \frac{\eta-\alpha\varepsilon}{1-\alpha\varepsilon}\right)\right] \frac{\partial c}{\partial \eta} +$$

$$+\alpha^2 K \left[\cos^4\left(\frac{\pi}{2}\,\frac{\xi-\alpha\varepsilon}{1-\alpha\varepsilon}\right) \frac{\partial^2 c}{\partial \xi^2} + \cos^4\left(\frac{\pi}{2}\,\frac{\eta-\alpha\varepsilon}{1-\alpha\varepsilon}\right) \frac{\partial^2 c}{\partial \eta^2}\right], \quad \text{for } |\xi| \geq \alpha\varepsilon.$$

Case (4) is essentially the same with $\varepsilon=1$.

For specific applications of the pseudospectral integrator, additional modifications were designed. These modifications addressed two general areas: specialized boundary conditions and judicious combinations of the Fourier expansion series. The first was aimed at reducing the aliasing errors when the signal crossed the boundaries and the second facilitated the various filtering algorithms. Both are the subject of ongoing research and lie outside the scope of the evaluation methodology. Although some sample results will be presented, details of these modifications will not be described.

The time discretization of the pseudospectral integrator was accomplished with the "leapfrog" algorithm:

$$C^{n+1} = C^{n-1} + 2\,\Delta t \left.\frac{\partial c}{\partial t}\right|^n \tag{7}$$

THE NEROS INTEGRATOR

The solution of the dispersion equation by the bi-directional polynomial (Lamb, 1983) is an extension of the quasi-Lagrangian advective scheme used by several modelers (Krishnamurti, 1962; Mahrer and Pielke, 1978; Bates and McDonald, 1982). For a pure advective problem the technique involves the upstream integration along a particle trajectory. For the one-dimensional case the solution of the advective equation,

$$\frac{\partial c}{\partial t} + u \frac{\partial c}{\partial x} = 0 \tag{8}$$

from time t_0 to t can be written as,

$$c(x,t) = \int c(x',t_0)\delta(x-x'-\overline{x})dx' \ , \tag{9}$$

where the integration is over all x' and

$$\overline{x} = \int_{t_0}^{t} u(x,t')dt' \ . \tag{10}$$

The delta function in equation (9) is the Green's function of equation (8).

The "Lamb" extension of this technique involved replacing the advective operator in equation (8) by an operator describing the advection and diffusion processes, yielding

$$\frac{\partial c}{\partial t} + u\frac{\partial c}{\partial x} - K \frac{\partial^2 c}{\partial x^2} = 0 \ . \tag{11}$$

The Green's function in this case is

$$g(x,t|x',t0) = \frac{1}{\sqrt{2\pi}\,\sigma} \exp\left[-\frac{1}{2\sigma^2}(x-x'-\overline{x})^2\right] \ , \tag{12}$$

where $\sigma^2 = 2Kt$; $\bar{x}$ is the same as in (10). The solution is

$$c(x,t) = \int c(x',t_0)g(x,t|x',t_0)dx' \ . \qquad (13)$$

Interpolating polynomials are used to define the interpolant space fields at time t_0. Substitution of the polynomials into equation (13) along with the use of (12) allows an analytical solution. For example, for a quadratic polynomial we have,

$$c(x,t) = a_0 - \tilde{x}a_1 + (\sigma^2 + \tilde{x}^2)\, a_2 \ , \qquad (14)$$

where $a_i (i=0,1,2)$ are the coefficients of the interpolating polynomial and $\tilde{x}$ is the distance to the nearest gridpoint. To construct an updated concentration field using (14) is straightforward. Generalization of the method to two dimensions and higher order polynomials is also straightforward, especially realizing that a polynomial substitution for $c(x',t_0)$ in (13) and the gaussian form of the Green's function of (13) show the solution of (13) to be the moments of a normal random variable.

This upstream Lagrangian technique provides the benefit of unconditional stability (Bates and McDonald, 1982). As with most numerical methods, the accuracy of this scheme increases with higher order approximations. This translates to increased computational costs due to more elaborate numerical operations and greater complexity in the formulation of the boundary conditions. For the comparisons presented in this report, a biquintic polynomial approximation was employed. The boundary conditions are specified by setting the concentration field to zero for inflow conditions and setting the normal derivative of the concentration field at the boundary to zero for outflow conditions.

The use of bidirectional approximations provides a matrix of gridpoint values feeding information to the desired solution. The order of the polynomial approximation employed determines the extent of surrounding gridpoint values used. In most numerical schemes, only the gridpoints in one direction are involved in the expression of derivatives in that direction; this would

be equivalent to neglecting all the cross-product terms in the polynomial representation. However, this shortcoming is unimportant in most explicit schemes which are limited by time step stability restrictions. Furthermore, care must be taken not to abuse the unconditional stability feature of the polynomial scheme because the travel of a particle over a distance greater than a grid distance over a time step will result in considerable accuracy deterioration.

It should be emphasized that this method requires regularly spaced grid-points. As will be mentioned later, this is not particularly restrictive for horizontal transport. For cases of varying grid sizes, e.g., in the vertical, coordinate transformations are possible.

3. EVALUATION METHODOLOGY AND TEST CASES

As mentioned in the Introduction, we have questioned the use of the uniform rotation of a gaussian puff as a benchmark in the evaluation methodology. It is felt that this test may be particularly advantageous for those integrators which rely on spectral-type expansions. Extensive experimentation with the pseudospectral integrator has revealed that the "worst" circumstances are associated with the signal approach and crossing of the boundaries. The solid body rotation of a puff would keep it a safe distance from the boundary unless the center of rotation is chosen away from the center of the mesh (Lamb, 1984). Moreover, the Fourier expansion of a gaussian signal produces a rather unique distribution in wave-number space (uniform) and consequently may produce unrepresentative results. The presented test cases attempt to eliminate these biases and produce a "fairer" evaluation methodology. It is conceivable that these test cases introduce biases of their own and perhaps favor a certain class of integrators. In the final analysis an exhaustive evaluation methodology should include a wide spectrum of test cases, with emphasis on realistic situations, and conclusions should be based on overall performance. For highly specialized applications it may be sufficient to concentrate on a narrower range of criteria.

The fundamental equation of advection-diffusion of atmospheric pollutants is,

$$\frac{\partial c}{\partial t} + \bar{U} \cdot \nabla c = K \nabla^2 c + Q \ , \qquad (15)$$

subject to appropriate boundary and initial conditions. c is the concentration, $\bar{U}$ is the advective velocity, K the diffusivity, and Q the emission rate. The following conditions have been assumed:

a. Two-dimensional fields, i.e., $\partial/\partial z = 0$. In fact, most air pollution models handle the vertical direction separately, either by decoupling the solutions or layer averaging. This may justify limiting the evaluation to horizontal transport simulations.

b. Constant, uniform advective velocity ($\bar{U}$ = const). Although it may be desirable to consider circumstances with variable advective velocities, the inherent complexities of obtaining exact analytical solutions to the transport equations prohibit such undertakings. Even with $\bar{U}$ = const., however, care must be taken in selecting representative situations. For example, it was discovered that for the pseudospectral integrator the use of a "diagonal" velocity (u = v = const.) produced unrealistically better results compared with the general case ($u \neq v$).

c. Constant, uniform diffusivity (K = const.). No real benefit is envisioned in varying this quantity spatially.

TEST CASES

We considered two basic test cases, the transport of a single puff and the constant point source. A limiting factor in the choice of the appropriate test case was the determination of the exact analytical solution, preferably in closed form. As will be demonstrated later, estimating the accuracy of the numerical integrator hinges on the knowledge of the analytical solution.

Single Puff. Assume the following initial condition:

$$Co(x,y) = \begin{cases} (2|x|^3-3x^2+1)(2|y|^3-3y^2+1) & , \ |x| \leq 1 \ , \ |y| \leq 1 \ . \\ 0 & , \ |x| \geq 1 \ , \ |y| \geq 1 \ . \end{cases} \tag{16}$$

This will be referred to as the "spline" puff. Figures 1 and 2 show the puff on the pseudospectral grid and a uniform grid, respectively. It should be emphasized that the function and its first derivatives are continuous on $|x|=1$ and $|y|=1$. The solution of (7) given the above initial condition and

PSEUDO-SPECTRAL

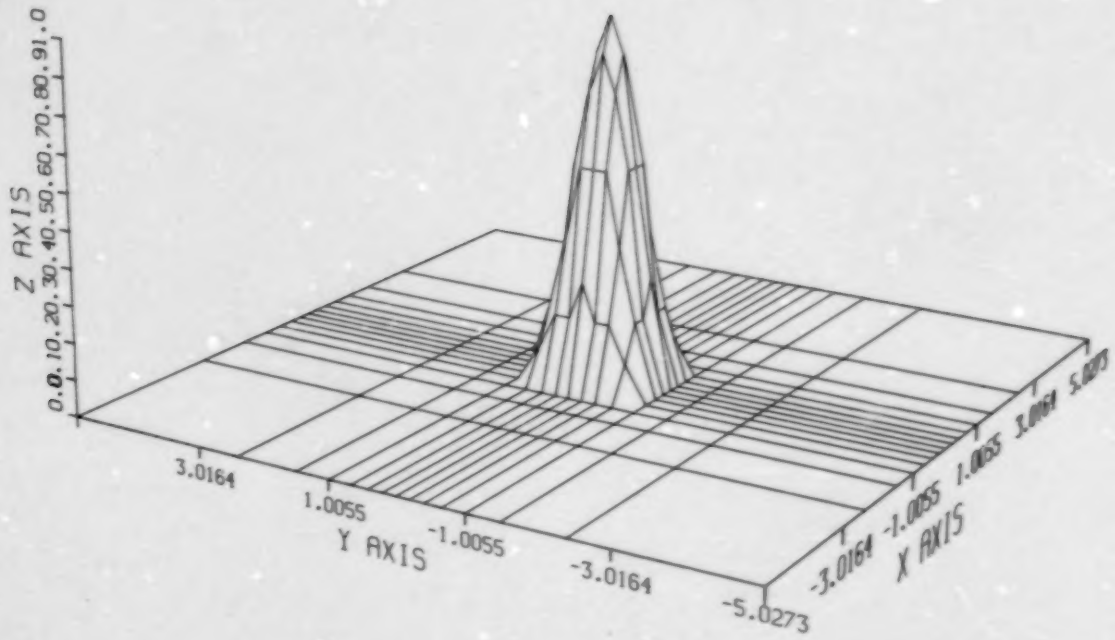

Figure 1.

BI-QUINTIC

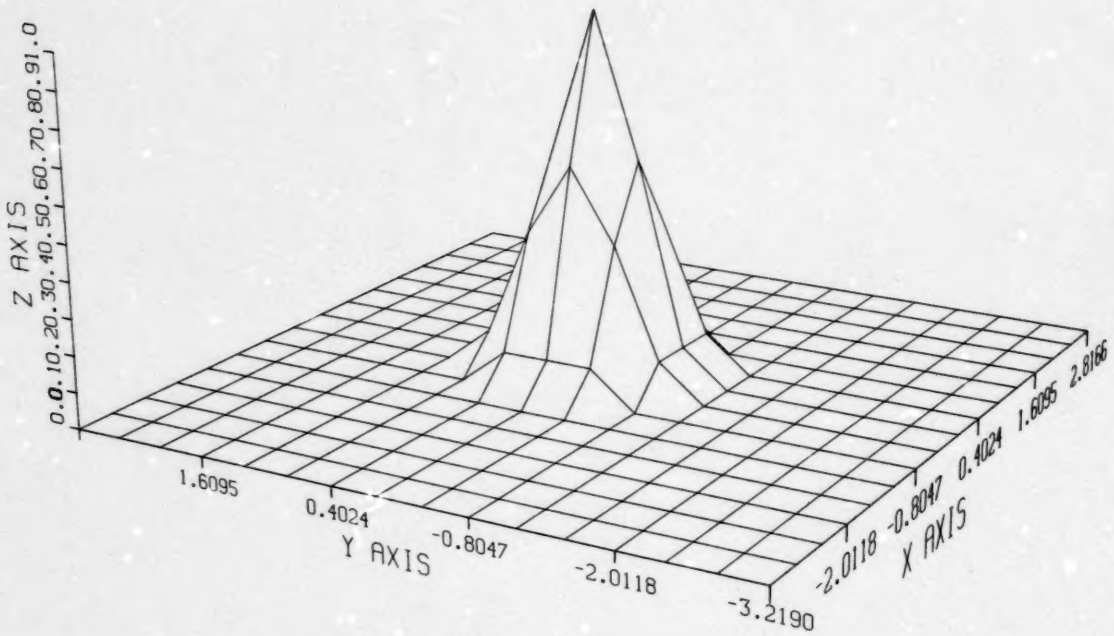

Figure 2.

Q=0 may be obtained using the Green's function approach. The resultant integral may be evaluated by separation of variables yielding,

$$C(x,y,t) = \frac{1}{\pi} A_x A_y \quad . \tag{17}$$

The quantity A_i (i=x,y) involves a series of exponentials and error functions. It will be presented for i=x; the i=y case would be similar.

Assume the following quantities:

$$\begin{aligned} \delta &= \sqrt{Kt} \\ x' &= x-ut \\ \omega_{1x} &= -\frac{x'}{2\sqrt{Kt}} \\ \omega_{2x} &= \frac{1-x'}{2\sqrt{Kt}} \\ \omega_{3x} &= \frac{-1-x'}{2\sqrt{Kt}} \quad , \end{aligned} \tag{18}$$

then,

$$\begin{aligned} A_x = {} & 8\delta^3\left(2\omega_{1x}^2 e^{-\omega_{1x}^2} - \omega_{2x}^2 e^{-\omega_{2x}^2} - \omega_{3x}^2 e^{-\omega_{3x}^2}\right) + 24\delta^2 x' \omega_{1x} e^{-\omega_{1x}^2} - 6\delta^2(2x'-1)\omega_{2x} e^{-\omega_{2x}^2} + \\ & - 6\delta^2(2x'+1)\omega_{3x} e^{-\omega_{3x}^2} + 4\delta\left(4\delta^2+3x'^2\right)e^{-\omega_{1x}^2} - 2\delta\left(4\delta^2+3x'^2-3x'\right)e^{-\omega_{2x}^2} + \\ & - 2\delta(4\delta^2+3x'^2+3x')e^{-\omega_{3x}^2} - 2\sqrt{\pi}\, x'(6\delta^2+x'^2)\operatorname{erf}(\omega_{1x}) + \frac{\sqrt{\pi}}{2}\left[6\delta^2(2x'-1)\right. \\ & \left. + 2x'^3-3x'^2+1\right]\operatorname{erf}(\omega_{2x}) + \frac{\sqrt{\pi}}{2}\left[6\delta^2(2x'+1)+2x'^3+3x'^2-1\right]\operatorname{erf}(\omega_{3x}) \quad , \end{aligned} \tag{19}$$

where erf(a) is the error function of a.

Constant Point Source. Assume that the point source of strength Q_0 is located at the origin of the coordinate system and the following initial condition, Co(x,y)=0. Equation (7) becomes,

$$\frac{\partial c}{\partial t} + \bar{U} \cdot \nabla c = K\nabla^2 c + Q_0\, \delta(x)\delta(y) \qquad (20)$$

where δ is the delta function.

Employing the Green's function approach we can derive the exact solution in integral form:

$$c(x,y,t) = \exp\left(\frac{x'u+y'v}{2K}\right) \int_0^{\omega} Q_0 \exp\left[-\frac{\sqrt{x'^2+y'^2}\,\sqrt{u^2+v^2}}{2K}\left(s+\frac{1}{s}\right)\right] \frac{ds}{4\pi K s}, \qquad (21)$$

where $x' = x-ut$

$y' = y-vt$

$$\omega = \frac{\sqrt{u^2+v^2}\; t}{\sqrt{x'^2+y'^2}}$$

The exact analytical solution cannot be easily derived in closed form. However, since the employed time steps in the numerical calculations are usually small, a simple numerical approximation of (21) was shown to be adequate. The steady-state solution of (20) and the asymptotic form of (21) is, of course, the gaussian solution.

PERFORMANCE CRITERIA

Accuracy. This is perhaps the most important criterion in the evaluation of any numerical integrator. It measures how well the numerical solution approximates the exact analytical solution. Measures of accuracy will depend on the values at the various gridpoints. We have identified three such measures borrowed from the nomenclature of applied mathematics. They are the norms L_1, L_2, and L_∞. These norms are computed using the numerical solution values at a set of gridpoints, S, and the exact solution values at

the same set of gridpoints. It is possible that the set of gridpoints includes all meshpoints; for some cases, however, it may be desirable to limit the norm estimates to a subset of the meshpoints.

L_1 is the sum, over S, of the absolute values of the deviations of the numerical solution values from the exact solution values. L_2 is the square root of the sum of the squares of these deviations. Both L_1 and L_2 are measures of the global performance of the numerical scheme. L_∞ is the maximum absolute value deviation observed over S. Although not useful for overall performance characterization, L_∞ is relevant for circumstances where the forecasting of peak values becomes particularly important.

Since the air pollution problems under consideration are time dependent the above mentioned norms vary with each time step and consequently it is often desirable to provide information on their variability with time. This may reveal special circumstances of deteriorating accuracy, e.g., the approach of the signal to the boundaries, failure to resolve developing steep gradients, etc.

Conservation. The conservation of total material in air pollution simulations is an important gauge of scheme performance. Although this property is related to accuracy it often depends on the manner in which the differential equations are derived (conservative or nonconservative form) and discretized. As will be shown, both schemes demonstrated reasonable conservation characteristics. However, the pseudospectral one with its deteriorating accuracy close to the boundaries presented some problems when the signal crossed the boundaries. This is particularly acute since the numerical estimation of the relevant integral quantity (total material) weights the outer points more heavily. It is recommended that conservation be investigated over the inner mesh core particularly when this inner grid is uniform.

Efficiency. All evaluation tests were performed on the CDC 7600 of Brookhaven National Laboratory, under the regular priority. Every possible effort has been made to insure that both schemes were subjected to similar operational procedures. This usually entailed similar areal coverage, similar time steps, and similar parameters. Results will be presented in terms of the corresponding computer resource units.

4. PRESENTATION OF RESULTS

Most computer test runs were conducted within the framework of the evaluation methodology described in earlier sections. Considerable effort was devoted to recognizing the important parameters affecting the performance of the two numerical schemes. This often involved repetitive simulations with incremental changes in the parameters under investigation. Although these "tours in parameter space" have by no means been exhaustive, it is felt that all important characteristics of the relevant parameters have been identified. In the folowing sections, representative results from the various test runs will be presented. They will be often accompanied by qualitative discussions of performance and its dependence on physical and computational parameters.

Most test runs were performed on a 16x16 mesh; the employed FFT routine performs optimally on a grid size which is a power of 2. As mentioned earlier, we will not dwell on the various attempts to improve the pseudo-spectral integrator. However, sample results from one such attempt will be presented. This has been employed for the case of the simply expanding mesh, transformation (2), and utilizes the convenience of performing the multiplication, e.g.,

$$\cos^2\left(\frac{\pi}{2}\,\xi\right)\frac{\partial c}{\partial \xi}\,, \tag{22}$$

in spectral space rather than real space. For a function $F(\xi)$ defined on $[-1,1]$ assuming a grid of $2N$ points we have,

$$F\left(\frac{j}{N}\right) = \sum_{k=-N}^{N-1} \hat{F}(k)\, e^{\frac{2\pi i k j}{2N}}\,, \quad j=-N, \ldots, N-1 \tag{23}$$

where $i = \sqrt{-1}$, and $\hat{F}(k)$ is the Fourier transform of F.

The derivative of F is

$$F'\left(\frac{j}{N}\right) \sim \sum_{-N}^{N-1} i\pi k\, \hat{F}(k) e^{\frac{i\pi kj}{N}} = \sum_{-N}^{N-1} \hat{G}(k) e^{\frac{i\pi kj}{N}} \qquad (24)$$

The expression (22) becomes

$$\cos^2\left(\frac{\pi j}{2N}\right) F'\left(\frac{j}{N}\right) = \frac{1}{2}\left[1 + \frac{1}{2}\left(e^{\frac{i\pi j}{N}} + e^{-\frac{i\pi j}{N}}\right)\right] \sum_{-N}^{N-1} \hat{G}(k)\, e^{\frac{i\pi kj}{N}}$$

$$= \sum_{k=-N}^{N-1} \left\{\frac{1}{2}\hat{G}(k) + \frac{1}{4}\left[\hat{G}(k-1)+\hat{G}(k+1)\right]\right\} e^{\frac{i\pi kj}{N}} , \qquad (25)$$

where the periodic extension of $\hat{G}$ must be used, i.e.,

$$\hat{G}(-N-1) = \hat{G}(N-1) , \quad \hat{G}(N) = \hat{G}(-N) . \qquad (26)$$

Apart from the resource unit savings of performing operations (22) in spectral space, it was determined that improvements in accuracy were realized by adjusting the highest wave number coefficients prior to implementing operation (25). This may be interpreted as a form of filtering. The results presented will be limited to the simple adjustment of a change in sign. Separate parametric investigations have determined that the optimum adjustments are problem-dependent and indeed may have to vary during the course of the calculation. The "simple" adjustment results will be referred to as SPMT. The straightforward pseudospectral case will be abbreviated as PS; the NEROS integrator as BQ.

ADVECTION-DIFFUSION/SPLINE PUFF

Consider the case u=v=1 with a diffusivity K=0.1 and the puff initially situated at the origin of the coordinate system (I=9, J=9). Assume the orginal transformation [equation (2)] for the pseudospectral integrator. The

bottommost gridline (I=1, ..., 16, J=1) and leftmost gridline (I=1, J=1, ...16) correspond to $-\infty$. An important parameter to be chosen is the grid-spacing for BQ. This choice was made on the basis of the subset of gridpoints, S, over which the norms were computed. For most cases, S was chosen to be the domain (I=3, ..., 15; J=3, ..., 15) which translates into ($-2.41 \leq x \leq +2.41$, $-2.41 \leq y \leq +2.41$) in real space. The areal coverage of S for both schemes should be the same, therefore, for BQ we have,

$$\Delta x = \Delta y = \frac{\tan\left(\frac{\pi}{2} \cdot \frac{3}{4}\right)}{6} \cong 0.402 \ . \qquad (27)$$

For the first series of calculations a total of N=150 time steps was used. Only the pseudospectral scheme has stability restrictions on the value of the employed time step: the standard restrictions of all explicit schemes (Roache, 1976). A time step of $\Delta t=0.01$ was initially used. Over the 150 time steps the center of the puff travelled a distance of

$$X = N \cdot \Delta t \cdot u = 150 \cdot 0.01 \cdot 1 = 1.5 \qquad (28)$$

along the x-axis (similarly for the y-axis). For the pseudospectral scheme this corresponds to gridpoint (I=J=14), while for BQ it is roughly halfway between gridpoint (I=J=11) and gridpoint (I=J=12). Clearly, for the pseudo-spectral scheme the puff has not approached the boundaries; gridpoint (16,16) corresponds to position (5.03,5.03). Table 1 presents the comparison of the norm statistics and the conservation results. The latter are computed over gridpoints (I=1, ..., 16; J=1, ..., 16). For BQ the total mass is estimated as,

$$T = \iint_D c(x,y)dxdy \cong \sum_{I=1}^{I=16} \sum_{J=1}^{J=16} c(I,J)\, \Delta x \Delta y \ . \qquad (29)$$

for the pseudospectral integrator because of the variable mesh the expression for the total mass is more complicated:

TABLE 1. SUMMARY OF RESULTS FOR SPLINE PUFF (INITIALLY AT ORIGIN), N=150, u=v=1, K=0.1, Δt=0.01

Integrator	Norm	$\bar{x}$ [a]	s [b]	Value of norm at time step 50	100	150	RU [c]
PS	L_1	0.263	0.038	0.27	0.25	0.34	
	L_2	0.035	0.009	0.031	0.032	0.06	
	L_∞	0.014	0.007	0.01	0.009	0.03	24.46 [d]
SPMT	L_1	0.273	0.046	0.29	0.26	0.24	
	L_2	0.033	0.004	0.031	0.033	0.034	
	L_∞	0.010	0.002	0.009	0.009	0.014	
BQ	L_1	0.214	0.061	0.28	0.21	0.15	
Δx=Δy=.402	L_2	0.036	0.01	0.046	0.036	0.025	43.65
	L_∞	0.016	0.005	0.021	0.018	0.012	

Conservation Results

	Total mass at time step 0	50	100	150
PS	0.995	1.000	0.998	0.949
SPMT	0.995	1.006	0.990	0.973
BQ	1.002	1.002	1.002	0.985

[a] Mean value over all time steps.

[b] Standard deviation over all time steps.

[c] Resource units.

[d] This value covers both PS and SPMT; for either one separately the value would be 60% of combined.

$$T = \iint_D c(x,y)dxdy = \frac{\pi^2}{4} \iint_D c(\xi,n) \frac{d\xi\ d\eta}{\cos^2(\frac{\pi}{2}\xi)\ \cos^2(\frac{\pi}{2}\eta)},$$

and is estimated as,

$$T \hat{=} \frac{\pi^2}{4} \sum_{I=2}^{I=16} \sum_{J=2}^{J=16} \frac{c(I,J)\ \Delta\xi\ \Delta\eta}{\cos^2[\frac{\pi}{2}(I-9)\Delta\xi]\ \cos^2[\frac{\pi}{2}(J-9)\Delta\eta]}. \qquad (30)$$

As mentioned earlier, the accuracy of the above expression deteriorates when the signal approaches the boundaries since the grid values of least accuracy contribute more to the estimate of the total mass.

On the basis of the comparisons in Table 1, performance of the three integrators is comparable although the pseudospectral ones are cheaper almost by a factor of 2. Conservation results are also comparable although the above mentioned deterioration may already be starting to appear. SPMT appears to be manifesting the optimum L_∞.

Table 2 presents equivalent results for K=0.01 and N=200. In general, decreasing the diffusivity by an order of magnitude appears to worsen all norms by the same order for all integrators. The ratio of resource units remains approximately the same as in Table 1; in fact, this ratio persists throughout all test runs. Noteworthy is the start of deterioration of the pseudospectral norms around time step 200 as the puff approaches the boundaries.

TABLE 2. SUMMARY OF RESULTS FOR SPLINE PUFF (INITIALLY AT ORIGIN), N=200, u=v=1, K=0.01, Δt=0.01

Integrator	Norm	$\bar{x}$	s	Value of norm at time step 50	100	150	200	RU
PS	L_1	1.507	0.978	0.72	1.6	1.6	4.0	
	L_2	0.199	0.131	0.09	0.21	0.23	0.50	
	L_∞	0.069	0.055	0.02	0.07	0.08	0.19	29.48[a]
SPMT	L_1	1.102	0.429	0.72	1.2	1.2	2.1	
	L_2	0.160	0.079	0.08	0.16	0.21	0.32	
	L_∞	0.054	0.034	0.02	0.05	0.09	0.10	
BQ	L_1	1.093	0.406	0.85	1.3	1.4	1.3	
$\Delta x=\Delta y=.402$	L_2	0.191	0.074	0.14	0.21	0.26	0.25	58.87
	L_∞	0.093	0.044	0.05	0.11	0.14	0.15	

Conservation Results

	Total mass at time step 0	50	100	150	200
PS	0.995	1.005	0.985	0.940	0.920
SPMT	0.995	1.010	0.982	0.965	0.932
BQ	1.002	1.002	0.999	1.015	0.989

[a]This value covers both PS and SPMT; for either one separately the value would be ~60% of combined.

Table 3 presents summary results from two cases with N=500. Although the puff is closer to the boundaries for the first case (compared with the case in Table 2), the higher diffusion produces superior norms. Nevertheless, BQ outperforms both PS and SPMT. For the second case, Δt is small; this condition clearly favors PS because ofthe lack of need for filtering coupled with the dense grid around the origin. In fact, filtering in this case produces inferior norms. Conservation exhibits similar results with Table 2 for the first case; for the second case all schemes perform satisfactorily.

TABLE 3. SUMMARY OF RESULTS FOR SPLINE PUFF (INITIALLY AT ORIGIN), N=500, u=v=1

Features	Integrator	Norm	$\bar{x}$	s	Value of norm at time step 100	200	300	400	500	RU
Δt=0.005	PS	L_1	1.226	0.661	0.56	1.1	1.3	2.4	1.1	
K=0.02		L_2	0.185	0.114	0.06	0.15	0.17	0.35	0.30	
		L_∞	0.093	0.089	0.01	0.06	0.06	0.15	0.25	
	SPMT	[a]L_1	0.928	0.312	0.55	0.89	0.92	1.4	1.1	70.0
		L_2	0.152	0.082	0.07	0.12	0.16	0.23	0.30	
		L_∞	0.071	0.071	0.02	0.03	0.07	0.08	0.24	
	BQ	L_1	0.806	0.271	0.74	1.0	1.1	0.84	0.45	
		L_2	0.142	0.045	0.12	0.17	0.18	0.16	0.10	138.6
		L_∞	0.066	0.027	0.05	0.08	0.10	0.10	0.04	
Δt=0.001	PS	L_1	0.185	0.043	0.23	0.23	0.18	0.16	0.16	
K=0.1		L_2	0.021	0.005	0.03	0.03	0.02	0.02	0.02	
		L_∞	0.005	0.002	0.01	0.01	0.004	0.003	0.003	70.3[a]
	SPMT	L_1	0.229	0.073	0.31	0.30	0.24	0.16	0.16	
		L_2	0.027	0.008	0.04	0.04	0.03	0.02	0.02	
		L_∞	0.006	0.002	0.01	0.01	0.01	0.004	0.004	
	BQ	L_1	0.311	0.124	0.20	0.31	0.38	0.43	0.43	
		L_2	0.05	0.017	0.03	0.05	0.06	0.06	0.06	138.7
		L_∞	0.014	0.005	0.01	0.02	0.02	0.02	0.02	

[a]This value covers both PS and SPMT; for either one separately the value would be ~60% of combined.

The next series of tests involves transformation (5) of the pseudo-spectral integrator which provides a uniform submesh. Atempts to develop a modification similar to SPMT were abandoned because of prohibitive complexities in the necessary algorithms. However, results of one simple

modification will be presented. This involved the imposition of a damping factor on the outer grid layer to reduce some of the developing oscillations. These results will be referred to as DF; results of the pseudospectral integrator with (5) will be referred to as PS5.

An important deficiency of the pseudospectral integrator was discovered during the tests with transformation (5). It was determined that the use of a diagonal velocity field (u=v=1) greatly improved the performance of the pseudospectral integrator. This improvement resulted in an average lowering of the norms of about 15% to 25%. This improvement was approximately the same for PS, SPMT, and for transformation (4). Although the exact reason for these changes may be difficult to ascertain, the speculation is that diagonal velocity fields creating symmetrical situations may cause the cancellation of certain error terms. BQ was, in fact, insensitive to the diagonality of the employed velocity field. A velocity field of u=0.25, v=1.0, was chosen as more representative.

Table 4 presents results of a case with N=200, K=0.025, and Δt=0.01. Transformation (5) introduces two additional parameters, α and ε. α controls the mesh size of the inner submesh and together with ε the total size of this inner submesh. Both ε and α were chosen to be 0.75. This results in an inner 9x9 uniform grid with grid size equal to 1/6. Using the same norm subspace S as with previous runs (I=3, ..., 15; J=3, ..., 15) the BQ grid size becomes $\Delta x=\Delta y \cong 0.174$. Although more costly, BQ is clearly superior to the pseudospectral integrators. The puff has almost totally exited the norm domain by time step 200. Both pseudospectral versions exhibited serious problems by that time, partly because of the asymmetric velocity field and partly because of the crossing of the boundary domain. The damping factor in DF improves this problem somewhat. It should be mentioned that attempts to improve the pseudospectral integrators by reducing the time step or increasing the number of meshpoints or both (keeping the cost equivalent to BQ) did not produce substantially improved results.

Table 5 presents summary results from a case where the focus is only on the inner 9x9 uniform submesh. All norms are computed only on this 9x9 subspace and the meshes are chosen to coincide exactly. For $\alpha=\varepsilon=0.75$ the grid space for BQ is $\Delta x=\Delta y= 1/16 \cong 0.166$. Only the DF version of the pseudo

TABLE 4. SUMMARY OF RESULTS FOR SPLINE PUFF (INITIALLY AT ORIGIN), N=200, u=0.25, v=1, K=0.025, Δt=0.01

Features	Integrator	Norm	$\bar{x}$	s	Value of norm at time step 50	100	150	200	RU
$\alpha=\varepsilon$=0.75	PS5	L_1	1.967	1.553	0.41	2.4	1.9	5.5	
		L_2	0.218	0.164	0.05	0.26	0.26	0.60	18.9
		L_∞	0.057	0.039	0.01	0.07	0.10	0.14	
	DF	L_1	1.383	0.780	0.41	2.4	1.8	2.2	
		L_2	0.170	0.098	0.05	0.26	0.25	0.28	19.2
		L_∞	0.050	0.031	0.01	0.07	0.09	0.08	
$\Delta x=\Delta y\cong 0.174$	BQ	L_1	0.091	0.031	0.09	0.14	0.04	0.07	
		L_2	0.015	0.006	0.01	0.02	0.01	0.02	56.6
		L_∞	0.006	0.003	0.003	0.01	0.002	0.01	

Conservation Results

	Total mass at time step 0	50	100	150	200
BQ	1.001	0.982	0.751	0.338	0.076

TABLE 5. SUMMARY OF RESULTS FOR SPLINE PUFF (INITIALLY AT ORIGIN) N=200, u=0.25, v=1, K=0.025, Δt=0.01

Features	Integrator	Norm	$\bar{x}$	s	Value of norm at time step 50	100	150	200	RU
$\alpha=\varepsilon$=0.75	DF	L_1	0.620	0.384	0.16	1.2	0.62	1.1	
		L_2	0.094	0.061	0.03	0.15	0.09	0.19	17.4
		L_∞	0.027	0.020	0.01	0.03	0.03	0.06	
$\Delta x\cong\Delta y$=0.166	BQ	L_1	0.028	0.012	0.04	0.04	0.02	0.01	
		L_2	0.004	0.002	0.01	0.01	0.003	0.003	56.5
		L_∞	0.001	0.0004	0.002	0.001	0.001	0.001	

Conservation Results

	Total mass at time step 0	50	100	150	200
DF	1.003	0.974	0.710	0.284	0.062
BQ	1.004	0.975	0.707	0.292	0.058

spectral was used. Although three times as expensive, BQ is clearly superior to DF. Furthermore, the norms of BQ decrease with increasing time step; the reverse is true for DF.

ADVECTION/SPLINE PUFF

The case of pure advection is perhaps the strictest of tests for numerical integrators; diffusion tends to smoothen gradients and facilitates their numerical representation, particularly for the pseudospectral integrators. Table 6 presents the results for a case with N=150, u=v=1, and Δt=0.01. These are equivalent to the results of Table 1 where the diffusivity was 0.1. All norms are considerably larger in the pure advection case, however, all three integrators perform similarly. The puff has yet to approach the boundaries. BQ is almost three times as expensive as PS or

TABLE 6. SUMMARY OF RESULTS FOR SPLINE PUFF (INITIALLY AT ORIGIN), N=150, u=v=1, K=0, Δt=0.01

Integrator	Norm	$\bar{x}$	s	Value of norm at time step 50	100	150	RU
PS	L_1	1.432	0.678	1.0	2.3	2.3	
	L_2	0.191	0.103	0.12	0.29	0.34	
	L_∞	0.058	0.039	0.02	0.09	0.12	14.2[a]
SPMT	L_1	1.179	0.401	0.96	1.7	1.9	
	L_2	0.162	0.073	0.11	0.22	0.31	
	L_∞	0.050	0.030	0.02	0.07	0.13	
BQ	L_1	1.261	0.592	0.96	1.5	2.1	
$\Delta x=\Delta y\cong 0.402$	L_2	0.212	0.102	0.16	0.26	0.36	39.1
	L_∞	0.098	0.055	0.06	0.13	0.20	

Conservation Results

	Total mass at time step 0	50	100	150
PS	0.994	1.003	1.003	0.915
SPMT	0.994	1.019	1.025	0.869
BQ	1.002	1.002	0.999	1.010

[a]This value covers both PS and SPMT; for either one separately the value would be ~60% of combined.

SPMT. BQ demonstrates better conservation properties than PS or SPMT as with previous cases.

Table 7 presents results equivalent to the results in Table 4. Noteworthy is the difference in resource units: BQ greater than the pseudospectral integrators by a factor of 5. Nevertheless, the differences in accuracy are striking. With the puff about to leave the domain, a sizable oscillatory "shadow" has developed in its wake for both pseudospectral integrators. Continuing the calculation ultimately leads to the growth of this "shadow" which swamps the entire mesh. For BQ, the puff departs the mesh with few residual oscillations. Again, attempts to improve PS5 or DF by reducing the time step or increasing the number of meshpoints (keeping total cost equivalent to that of BQ) were unsuccessful.

DIFFUSION/SPLINE PUFF

As mentioned earlier, diffusion contributes to a better performance, particulary for the pseudospectral integrators. Apart from the smoothing of the gradients, diffusion dampens the oscillations which plague the unfiltered pseudospectral integrator. In fact, as shown in Table 8, filtering contributes nothing to the pseudospectral norms. Results in Table 8 are equivalent to results in Table 1 (advection-diffusion) and Table 6 (pure advection). Also included in Table 8 are the BQ results for K=1.0; for emphasis it is mentioned that PS and SPMT are marginally unstable for that diffusivity: For a 2-D case of pure diffusion the condition on Δt is (Roache, 1976),

$$\frac{K\,\Delta t}{\Delta x^2_{min}} + \frac{K\,\Delta t}{\Delta y^2_{min}} \leq \frac{1}{2} . \qquad (31)$$

The smallest grid spacings are around the origin, thus

$$\Delta x_{min} = \Delta y_{min} = \tan\left(\frac{\pi}{2}\frac{1}{8}\right) \cong 0.1989 .$$

Condition (31) becomes

$$\Delta t \leq \frac{1}{2}\frac{0.1989^2}{2} = 0.00989 . \qquad (32)$$

TABLE 7. SUMMARY OF RESULTS FOR SPLINE PUFF (INITIALLY AT ORIGIN), N=200, u=0.25, v=1, K=0, Δt=0.01

Features	Integrator	Norm	$\bar{x}$	s	Value of norm at time step 50	100	150	200	RU
$\alpha=\varepsilon=0.75$	PS5	L_1	5.371	4.095	0.78	7.2	7.4	15	
		L_2	0.629	0.478	0.10	0.73	1.0	1.7	10.0
		L_∞	0.175	0.145	0.03	0.15	0.38	0.42	
	DF	L_1	4.875	3.458	0.78	7.2	7.0	7.3	
		L_2	0.590	0.425	0.10	0.73	1.0	1.1	10.1
		L_∞	0.174	0.145	0.03	0.15	0.39	0.35	
$\Delta x=\Delta y\cong 0.174$	BQ	L_1	0.438	0.164	0.32	0.65	0.33	0.34	
		L_2	0.062	0.026	0.04	0.09	0.05	0.07	51.7
		L_∞	0.020	0.010	0.01	0.03	0.02	0.03	

TABLE 8. SUMMARY OF RESULTS FOR SPLINE PUFF (INITIALLY AT ORIGIN), N=150, u=v=0, Δt=0.01

Features	Integrator	Norm	$\bar{x}$	s	Value of norm at time step 50	100	150	RU
K=0.05	PS	L_1	0.090	0.030	0.13	0.07	0.06	
		L_2	0.010	0.003	0.01	0.01	0.01	
		L_∞	0.002	0.001	0.002	0.001	0.001	23.5[a]
	SPMT	L_1	0.095	0.029	0.13	0.08	0.06	
		L_2	0.010	0.003	0.01	0.01	0.01	
		L_∞	0.002	0.001	0.002	0.001	0.001	
	BQ	L_1	0.158	0.038	0.18	0.18	0.15	
	$\Delta x=\Delta y=.402$	L_2	0.028	0.007	0.03	0.03	0.03	41.5
		L_∞	0.014	0.003	0.02	0.02	0.01	
K=1.0	PS	Unstable						
	SPMT	Unstable						
	BQ	L_1	0.132	0.117	0.02	0.15	0.41	
	$\Delta x=\Delta y=.402$	L_2	0.014	0.011	0.002	0.02	0.04	41.3
		L_∞	0.004	0.003	0.001	0.004	0.007	

[a]This value covers both PS and SPMT; for either one separately the value would be ~60% of combined.

Increased diffusivity does not necessarily improve the norms of BQ. From Table 8 it can be seen that higher K contributes to higher norms at the later time steps, even though the statistics show a general improvement. Differences between the pseudospectral and BQ resource units are the smallest compared with the cases of advection-diffusion and pure advection. The apparent superiority of PS and SPMT over BQ may be related to the denser grid around the origin where the puff remains. Table 9 presents similar results in Table 8 but with the puff situated at (1.0,1.0), BQ clearly outperforming PS and SPMT in this case.

TABLE 9. SUMMARY OF RESULTS FOR SPLINE PUFF [INITIALLY AT (1,1)], N=150, u=v=0, K=0.05, Δt=0.01

Integrator	Norm	$\bar{x}$	s	Value of norm at time step 50	100	150	RU
PS	L_1	0.225	0.081	0.20	0.28	0.31	
	L_2	0.047	0.017	0.05	0.06	0.06	
	L_∞	0.022	0.008	0.02	0.03	0.03	23.6[a]
SPMT	L_1	0.230	0.085	0.21	0.29	0.32	
	L_2	0.047	0.016	0.04	0.06	0.06	
	L_∞	0.021	0.008	0.02	0.03	0.03	
BQ	L_1	0.093	0.030	0.09	0.12	0.12	
$\Delta x=\Delta y=0.402$	L_2	0.017	0.006	0.01	0.02	0.02	43.2
	L_∞	0.008	0.003	0.01	0.01	0.01	

[a]This values covers both PS and SPMT; for either one separately the value would be 60% of combined.

ADVECTION-DIFFUSION/CONSTANT SOURCE

The case of the constant point source which leads to the formation of a steady-state plume is a serious test particularly for the pseudospectral integrators since it involves a continuous crossing of the boundaries. It appears that the customary filtering algorithms traditionally applied to the transport of an individual puff are inadequate for the plume simulations. It is likely that the judicious application of absorbing boundary layers (Christensen and Prahm, 1976) may alleviate some of the waviness in the computed solutions. Interestingly enough, these waves do not grow in time and

are not associated with the oscillations usually related to computational instability. They are the result of the schemes' inability to resolve the sharp gradients which develop on the plume borders and immediately upwind of the source. This problem is also present for BQ. Although for practical problems it may be advisable to devise specific remedies such as a finer mesh around the source or the spreading of the point source over several gridpoints, the results presented here represent "worst case" performance and are intended for comparison; no such improvements were attempted.

As with the case of the spline puff, "diagonal" velocities improve the norms of the pseudospectral integrators an average of 20%. For the results presented here a velocity of u=.25, v=1, was used. Table 10 presents results of a simulation with source strength Q_0=100, K=.025, and Δt=0.01. The norm domain S is (I=3, ..., 15; J=3, ..., 15) and the gridspacing for BQ is 0.402. The value of the concentration at the origin where the source is located is not included in the norm calculations. Although all three schemes appear comparable with the exception of L_1, it is important to emphasize that most of the errors in BQ were concentrated at the few gridpoints just upwind of the source where some exceptionally high negative values were computed.

TABLE 10. SUMMARY OF RESULTS FOR CONSTANT SOURCE (AT ORIGIN), N=200, u=0.025, v=1, K=0.25, Δt=0.01

Integrator	Norm	$\bar{x}$	s	Value of norm at time step 50	100	150	200	RU
PS	L_1	662	173.1	530	620	740	980	
	L_2	97.8	13.1	91	94	100	120	
	L_∞	41.3	5.4	42	36	43	47	
SPMT	[a]L_1	1012	208.7	910	1000	1200	1100	27.7
	L_2	134.5	15.7	130	140	150	140	
	L_∞	46.5	6.3	50	47	44	45	
BQ	L_1	494	121	454	496	495	487	
$\Delta x=\Delta y=.402$	L_2	98.2	12.8	92	102	104	102	53.4
	L_∞	59.5	13.8	67	62	65	63	

[a]This values covers both PS and SPMT; for either one separately the value would be 60% of combined.

The pseudospectral results showed more widespread waviness of lower amplitude. This is further confirmed by comparing L_∞ values which are lower for PS and SPMT. Clearly, SPMT fails in its filtering attempt. Conservation results are not included because of the inherent difficulties of estimating the contribution at the origin and the complications of the large negative concentrations. The latter problem remains a formidable one for most air pollution simulations and should be addressed in the future. Current remedies include periodic bookkeeping adjustments and zeroing of the negative values. This works reasonably well for BQ but fails with PS unless the resultant mass redistribution is carefully orchestrated to conform to certain Fourier transform rules.

Table 11 presents results of a simulation with transformation (5) for PS5 with $\alpha=\varepsilon=0.75$. The gridspacing for BQ is 0.174. The norm domain S is the same (I=3, ..., 15; J=3, ..., 15) and the damping factor algorithm DF is attempted for the pseudospectral integrator. Again, performance appears comparable; DF does not affect the solution over S and the patterns of waviness are similar to the previous case. The comparisons of resource units resemble those of the spline puff.

TABLE 11. SUMMARY OF RESULTS FOR CONSTANT SOURCE (AT ORIGIN), N=200, u=0.25, v=1, K=0.025, Δt=0.01

Integrator	Norm	$\bar{x}$	s	Value of norm at time step 50	100	150	200	RU
PS	L_1	630	166.6	550	570	840	770	
	L_2	101.8	16.3	98	97	120	110	15.8
	L_∞	46.3	6.2	45	44	52	46	
SPMT	L_1	629	166.9	550	560	840	760	
	L_2	101.7	16.3	98	97	120	110	15.9
	L_∞	46.3	6.2	44	44	52	47	
BQ	L_1	327.9	89.2	320	380	380	380	
$\Delta x=\Delta y=.174$	L_2	86.2	18.4	93	92	92	92	53.5
	L_∞	55.4	11.6	61	59	59	59	

Table 12 presents results similar to Table 11 but for K=0.1. A marked improvement in norms is noticed; this is particularly the case for BQ whose norms are all smaller than PS5 and DF by a factor of 2.

TABLE 12. SUMMARY OF RESULTS FOR CONSTANT SOURCE (AT ORIGIN), N=200, u=0.25, v=1, K=0.1, Δt=0.01

Integrator	Norm	$\bar{x}$	s	Value of norm at time step 50	100	150	200	RU
PS	L_1	117.7	12.8	110	130	130	120	
	L_2	20.2	2.7	19	20	19	19	15.7
	L_∞	10.3	2.5	9.7	9.6	9.3	9.0	
SPMT	L_1	118.3	13.1	110	130	130	120	
	L_2	20.2	2.7	19	20	19	19	15.8
	L_∞	10.3	2.5	9.7	9.6	9.3	9.0	
BQ	L_1	43.8	9.1	48	47	46	48	
$\Delta x=\Delta y=.174$	L_2	11.2	1.9	12	12	12	1	53.3
	L_∞	6.4	1.1	6.4	6.9	6.9	6.9	

5. CONCLUSIONS

A representative sample of the attempted test simulations has been presented. The following observations and conclusions summarize our views on the comparison of the two integrators and on the evaluation methodology in general.

1. A comprehensive evaluation methodology should include a variety of simulation tests such as the "solid body" rotation, transport across boundaries, point and areal sources, etc. The controlling factor in the particular test selection should be the availability of an exact solution preferably in analytical closed-form terms or in simple and verifiable numerical form. The puffs used in transport simulations should be of general shape and velocity fields should not be symmetric. Results of tests on the pseudospectral integrators, not included in this report, demonstrated unrealistically favorable results for the "solid body" rotation cases whenever the puff remained within the boundaries of the domain. Moreover, the use of a gaussian puff added to the advantage.

The use of the three "norms" (L_1, L_2, L_∞) for evaluating accuracy appears an acceptable approach. Use of the norms on subspaces of the domain permit a more selective evaluation of performance. In estimating the "conservaton of mass" property it is important to correctly account for flux terms across boundaries.

2. The NEROS integrator demonstrated a more consistent performance than the various versions of the pseudospectral integrator. This consistency was maintained throughout the different values of diffusivity and other parametric changes. Although more than twice as costly, it achieved superior accuracy particularly for simulations involving transport across mesh boundaries for which the pseudospectral integrators manifested serious problems. It should be emphasized that increasing the number of meshpoints, or decreasing the time step, for the pseudospectral integrators (to equate

cost to that of the NEROS) did not eliminate this problem. Higher diffusion was perhaps the best remedy for the pseudospectral problems; accuracy was considerably improved in this case. The NEROS integrator also improved with higher diffusion although not as pronounced. Higher diffusion, however, forces smaller time step restrictions on the pseudospectral integrator which is controlled by the diffusive constraints of explicit schemes. The NEROS integrator does not suffer these constraints because of its unconditional stability.

3. The pseudospectral integrator possesses several attractive features: the expanding mesh eliminates the periodicity problem and permits improved accuracy in areas of interest; accuracy is perhaps the optimum achieved among finite difference schemes. The attractive features have to be balanced against some of the problems of this scheme. As stated earlier, the most serious problem occurs when material crosses the mesh boundaries. This is related to the fact that by design the grid is quite sparse near the boundaries and the finite Fourier series expansion yields oscillatory fields which compromise the solution. Because of the finite Fourier series expansion, all gridpoint values contribute to the solution at each gridpoint. Although promoting superior accuracy, this feature is also a complication because localized filtering attempts are ineffective in reducing the "aliasing" errors. Efforts to implement the Kreiss and Oliger (1979) filter were unsuccessful. Only the simplest of filters (referred to as SPMT) which involved a simple manipulation of the highest wave number coefficients was consistently successful. A new filter, currently under study, involving expansions in terms of sines only is showing some promise but pays a penalty in reduced accuracy. Limited success was achieved with boundary damping factors.

The improved performance of the pseudospectral integrator for "diagonal" velocity fields (u=v) is another example of a somewhat erratic performance. In the final analysis all the pros and cons of this integrator have to be weighed for each specific application before it can be endorsed. The original pseudospectral integrator (Christensen and Prahm, 1976) with the conventional control methods [uniform mesh, absorbing boundary layers, reduction to periodicity (Roache, 1978)] may have more global applications.

4. The simulation of a point source emission leading to a steady-state plume is a particularly acute test case because of the sharp gradients across the plume boundaries and upwind of the source. The NEROS integrator produces some large negative values upwind of the source which are quite localized, however. In contrast, the pseudospectral integrators produce a more widespread oscillatory fields and no filtering algorithm has proven effective in this case.

5. An important point needs to be made regarding the efficiency of the numerical integrators. Current photochemical models as well as the envisioned acid deposition models are dominated by the chemical reaction simulations in terms of computer time demands; estimates of this demand average about 85% of total model requirements. It is essential to keep this in perspective in attempting to optimize the advection-diffusion integrator. The best integrator in this case may in fact be the one which allows better optimization of the chemical reaction simulations while maintaining reasonable standards of accuracy and conservation for the transport terms.

6. REFERENCES

Anderson, D., and B. Fattahi, 1974: A comparison of numerical solutions of the advective equation. J. Atmos. Sci., 31, 1500-1506.

Bates, J.R., and A. McDonald, 1982: Multiply-upstream, semi-Lagrangian advective schemes: analysis and application to a multi-level primitive equation model. Mon. Wea. Rev., 110, 1831-1842.

Chock, D.P., and A.M. Dunker, 1983: A comparison of numerical methods for solving the advection equation. Atmospheric Environment, 17, 11-24.

Christensen, O., and L.P. Prahm, 1976: A pseudo-spectral model for dispersion of atmospheric pollutants. J. Appl. Meteor., 15, 1284-1294.

Crowley, W.P., 1968: Numerical advection experiments. Mon. Wea. Rev., 96, 1-11.

Forester, C.K., 1977: Higher order monotonic convective difference schemes. J. Comput. Phys., 23, 1-22.

Fornberg, B., 1975: On a Fourier method for the integration of hyperbolic equations. SIAM J. Numerical Analysis, 12, No. 4, 509-528.

Fox, D.G., and S.A. Orszag, 1973: Pseudospectral approximation to two-dimensional turbulence. J. Comput. Phys., 11, 612-619.

Gazdag, J., 1973: Numerical convective schemes based on accurate computation of space derivatives. J. Comput. Phys., 13, 100-113.

Kreiss, H.O., and J. Oliger, 1979: Stability of the Fourier method. SIAM J. Numerical Analysis, 16, No. 3, 421-433.

Krishnamurti, T.N., 1962: Numerical integration of primitive equations by a quasi-Lagrangian advective scheme. J. of Appl. Meteor., 1, 508-521.

Lamb, R.G., 1983: A regional scale (1000 km) model of photochemical air pollution. Part I - Theoretical formulation. EPA-600/3-83-035, Environmental Protection Agency, Research Triangle Park, N.C.

Lamb, R.G., 1984: Personal communication.

Long Jr., P.E., and D.W. Pepper, 1976: A comparison of six numerical schemes for calculating the advection of atmospheric pollution. Third Symposium on Atmospheric Turbulence, Diffusion and Air Quality, 19-22 Oct. 1976, Raleigh, N.C., 181-187.

Long Jr., P.E., and D.W. Pepper, 1981: An examination of some simple numerical schemes for calculating scalar advection. J. Appl. Meteor., 20, 146-156.

Mahrer, Y., and R.A. Pielke, 1978: A test of an upstream spline interpolation technique for the advection terms in a numerical mesoscale model. Mon. Wea. Rev., 106, 818-830.

McRae, G.J., W.R. Goodin, and J.H. Seinfeld, 1982: Numerical solution of the atmospheric diffusion equation for chemically reacting flows. J. Comput. Phys., 45, 1-42.

Molenkamp, C.R., 1968: Accuracy of finite-difference methods applied to the advection equation. J. Appl. Meteor., 7, 160-167.

NCAR, 1983: Regional acid deposition: models and physical processes. NCAR/TN-214 + STR, Boulder, Co.

Patrinos, A.A.N., and M.J. Leach, 1982: One the use of pseudo-spectral technique in air-pollution modeling. Proceedings of the Third Joint Conference on Applications of Air Pollution Meteorology, 1982, San Antonio, Tx., 98-101.

Roache, P.J., 1972: Computational Fluid Dynamics. Hermosa Publishers, Albuquerque, N.M.

Roache, P.J., 1978: A pseudospectral FFT technique for nonperiodic problems. J. Comp. Phys., 27, 204-220.

Schere, K.L., 1983: An evaluation of seveal numerical advection schemes. Atmospheric Environment, 17, 1897-1907.

Wengle, H., and J.H. Seinfeld, 1978: Pseudospectral solution of atmospheric diffusion problems. J. Comp. Phys., 26, 87-106.